Diamond & Related Materials 166 (2026) 113687

Contents lists available at ScienceDirect

Diamond & Related Materials

journal homepage: www.elsevier.com/locate/diamond

Stacking-tunable electronic properties in recently synthesized hydrogen-substituted graphdiyne

Guilherme S.L. Fabris [a], Raphael B. de Oliveira [b], Bruno Ipaves [a], Marcelo L. Pereira Junior [b,c,*], Douglas S. Galvão [a,**]

[a] Applied Physics Department and Center for Computational Engineering & Sciences, State University of Campinas, Campinas, São Paulo 13083970, Brazil
[b] Department of Materials Science and NanoEngineering, Rice University, Houston, TX 77005, USA
[c] University of Brasília, College of Technology, Department of Electrical Engineering, 70910-900, Brasília, Federal District, Brazil

ARTICLE INFO

Keywords:
Graphynes
Graphdiynes
Hydrogenation
DFT
Electronic and optical properties

ABSTRACT

Recent progress in porous carbon materials has highlighted the importance of structural design in controlling emergent physicochemical properties. In this context, hydrogen-substituted graphdiyne (HsGDY), a three-dimensional framework derived from graphdiyne, has recently emerged as a promising architecture whose stacking-dependent behavior remains largely unexplored. Here, we present a comprehensive first-principles investigation of the structural, electronic, and optical properties of HsGDY across distinct stacking sequences. Our calculations identify the AA and ABC configurations as the most energetically favorable, with AA corresponding to the global minimum consistent with recent experimental observations. Electronic-structure analysis with both semilocal and screened hybrid functionals indicates that HsGDY is an indirect semiconductor. For the highly stable AA configuration, the fundamental band gap reaches 1.37 eV at the HSE06 level. This semiconducting behavior is primarily driven by modifications to the π-conjugated carbon network and by lattice symmetry breaking, rather than by direct hydrogen orbital contributions. The optical response exhibits pronounced absorption features spanning the visible to ultraviolet regions highlighting strong potential for optoelectronic applications. *Ab initio* molecular dynamics simulations at 700 K confirm the thermal robustness of the framework with negligible structural distortions. Collectively these findings elucidate the stacking dependent stability and semiconducting character of HsGDY providing a solid theoretical foundation for its integration into next generation nanoelectronic and energy harvesting technologies.

1. Introduction

Recent advances in carbon-based nanomaterials have underscored the central role of hybridization-driven structural design in tailoring physicochemical properties for next-generation nanoelectronics, energy-storage, and optoelectronics technologies [1–3]. The coexistence of sp, sp^2, and sp^3 hybridization states enables the formation of allotropes with markedly distinct structural and functional properties, positioning carbon at the forefront of modern materials science. Following the discovery of graphene in 2004 [4], extensive efforts have been devoted to identifying other carbon allotropes capable of overcoming graphene's intrinsic electronic zero band gap, which limits its applicability in semiconductor devices requiring high on-off current ratios [2,3], while retaining some of graphene's properties.

Graphynes (GYs) and graphdiynes (GDYs) constitute an important class of two-dimensional (2D) carbon allotropes formed by replacing C–C bonds in graphene with acetylenic (–C≡C–) or diacetylenic (–C≡C–C≡C–) linkages, yielding planar networks composed of mixed sp and sp^2 hybridized carbon atoms [3]. Graphyne was theoretically proposed by Baughman and co-workers in 1987 as a family of crystalline carbon allotropes with high sp content [2,5]. Although extended graphyne sheets remain experimentally challenging to synthesize [6–8], α-graphdiyne (α-GDY) was successfully fabricated in 2010 through *in situ* cross-coupling of hexaethynylbenzene monomers on copper foil [3,9,10], marking the transition from theoretical predictions to experimentally accessible porous carbon frameworks. Other graphyne-based structures, such as nanotubes [11,12] and scrolls [13] are also possible.

α-GDY exhibits remarkable properties arising from its sp-sp^2 conjugated structure with uniformly distributed intrinsic nanopores with diameters of approximately 5–6 Å. First-principles calculations predict a direct electronic band gap of approximately 0.44–1.47 eV for a monolayer, offering a significant advantage over graphene [10,14,15]. The electronic band gap can be further tuned through strain,

* Corresponding author at: University of Brasília, College of Technology, Department of Electrical Engineering, 70910-900, Brasília, Federal District, Brazil.
** Corresponding author.
E-mail addresses: marcelo.lopes@unb.br (M.L. Pereira Junior), galvao@ifi.unicamp.br (D.S. Galvão).

https://doi.org/10.1016/j.diamond.2026.113687
Received 14 February 2026; Received in revised form 14 April 2026; Accepted 16 April 2026
Available online 2 May 2026

chemical doping, nanoribbon engineering, and functionalization [10,15,16]. Moreover, charge carriers may reach mobilities on the order of 10^5 cm^2 V^{-1} s^{-1}, and the material has been synthesized in multiple morphologies, including nanosheets, nanowires, nanotubes, and three-dimensional (3D) porous structures [10,17]. These characteristics have enabled the exploration of graphdiyne-based systems in catalysis, sensing, energy storage, photocatalysis, and biomedical applications [10,15].

A recent experimental breakthrough is the synthesis of hydrogen-substituted graphdiyne (HsGDY) with a highly ordered AA-stacked structure, achieved via scalable thermal and chemical methods [18,19]. This architecture demonstrates that hydrogen substitution combined with controlled interlayer stacking can significantly enhance lithium adsorption and diffusion through well-defined pore channels, leading to reversible capacities exceeding 1000 mAh g^{-1}. Despite this progress, the stacking-dependent physicochemical properties of HsGDY remain insufficiently understood at the atomistic level, particularly with respect to the interplay between hydrogen functionalization and interlayer registry.

In this work, we have carried out a systematic first-principles investigation of HsGDY. While the experimentally synthesized AA stacking is used as the primary reference, alternative AB and ABC stacking configurations are also examined to evaluate their relative energetic stability and to clarify the influence of interlayer registry on structural, electronic, optical, and mechanical properties. This approach establishes a coherent framework for connecting experimentally observed structures with stacking-dependent trends, providing nanoscale insights into the roles of hydrogen functionalization and interlayer arrangement in this emerging porous carbon material.

2. Methodology

The structural stability and electronic and optical properties of HsGDY were investigated using *ab initio* simulations within the framework of Density Functional Theory (DFT) [20] as implemented in the SIESTA code [21,22]. Exchange–correlation effects were described using the nonlocal van der Waals density functional of the optB88-vdW type, also referred to as the vdW/KBM functional [23], selected for its demonstrated accuracy in describing dispersion-driven interactions in layered materials. A double-ζ polarized (DZP) numerical atomic orbital basis set was employed due to its proven reliability in accurately representing carbon-based hybrid frameworks [24]. A real-space mesh cutoff of 450 Ry was adopted together with a Γ-centered Monkhorst–Pack grid [25] of $3 \times 3 \times 6$ k-points for the primitive cell, whereas a $2 \times 2 \times 4$ grid was used for stacking calculations. All computational parameters were carefully tested to ensure the convergence of total energies and derived properties. To address the well-known band-gap underestimation typical of semilocal density functionals, single-point energy calculations were subsequently performed on the vdW/KBM optimized structures using the Heyd–Scuseria–Ernzerhof (HSE06) screened hybrid functional [26]. These hybrid calculations were carried out using the Hefei Order-N Packages for Ab initio Simulations (HONPAS) package [27,28], employing the same basis set and reciprocal-space sampling to ensure a consistent and highly accurate description of the electronic structure.

All structures were fully relaxed until the maximum residual force on each atom was lower than 0.01 eV/Å, and the total energy convergence threshold for the self-consistent field cycle was set to 10^{-6} eV. Spin-unpolarized calculations were performed in accordance with the observed nonmagnetic character of the systems under investigation.

Thermal stability was assessed through *ab initio* molecular dynamics (AIMD) simulations performed in the canonical ensemble using the Velocity-Verlet integration scheme combined with a Nosé–Hoover thermostat [29]. Each system was equilibrated for 10 ps with a time step of 1 fs at 700 K, while total energy fluctuations and atomic displacements were continuously monitored throughout the simulations to rigorously confirm the structural integrity under finite temperatures.

Structural dynamical stability was further evaluated through phonon dispersion calculations based on the density-functional tight-binding (DFTB) approach as implemented in the DFTB+ package [30–33], using an established parametrization together with the Phonopy code [34]. The calculations were performed on a $2 \times 2 \times 3$ supercell to ensure an adequate description of the lattice dynamics of bulk HsGDY. The strict absence of imaginary frequencies in the calculated dispersion relations provides definitive confirmation of the dynamical stability. This combined computational framework provides a consistent and reliable basis for assessing the thermodynamic and dynamical structural stabilities prior to interpreting the physical properties discussed in the following sections.

3. Results and discussion

This section presents a systematic analysis of the structural and physicochemical properties of hydrogen-substituted graphdiyne, with particular emphasis on the role of stacking configurations in determining its stability and electronic behavior. The discussion is organized to establish a clear structure–property relationship, beginning with the identification of the most favorable stacking arrangements, followed by an assessment of their energetic and dynamical stability. Subsequently, the electronic and optical responses are examined to elucidate how interlayer registry influences the functional characteristics of this layered porous carbon framework.

3.1. Crystal structure and stacking configurations

We first establish the structural models of α-GDY, γ-GDY, and HsGDY and define the stacking registries used throughout this work. As reported in recent experimental syntheses [18,19], the HsGDY architecture can be conceptualized as a derivative of the pristine γ-GDY phase. In the standard γ-GDY framework, each hexagonal ring is connected to six adjacent rings via acetylenic linkages. To construct the HsGDY lattice, three alternating acetylenic chains along with their connected hexagons are removed. The remaining unsaturated carbon atoms on the central ring are then passivated with hydrogen atoms. Fig. 1 illustrates these structural relationships and the detailed atomic substitutions. Alternatively, the HsGDY structure can be geometrically mapped onto the simpler α-GDY lattice. In this analogy, the sp^2-hybridized carbon atoms of the α-GDY phase are selectively replaced by benzenoid rings with the open valences saturated by hydrogen.

The layered crystals are built by stacking individual sheets along the out-of-plane direction, in close analogy with graphite, where interlayer cohesion is primarily governed by van der Waals interactions. Following the structural characterization from recent experimental synthesis [18,19], the AA stacking corresponds to a direct vertical replication of the system. In this arrangement, all atoms interact directly with their exact images in the adjacent sheets. In addition to the experimentally reported AA arrangement the AB and ABC registries are considered to facilitate a consistent discussion of stacking-dependent trends in the subsequent sections. In the AB configuration, the hexagonal ring of the upper layer is positioned exactly above the center of the larger pore of the underlying HsGDY sheet. This site corresponds to the location where another hexagonal ring would have originally resided in the parent γ-GDY framework. The ABC stacking follows a periodic sequence but introduces three distinct relative layer positions. In this arrangement, the hexagons of each successive sheet are consistently placed over the pore of the preceding layer. Unlike the AB configuration, the ABC stacking completely fills the projected empty spaces of the porous network when viewed along the stacking axis. Fig. 1 summarizes the in-plane hexagonal lattices of both materials and illustrates the relative layer registries associated with the AA, AB, and ABC sequences.

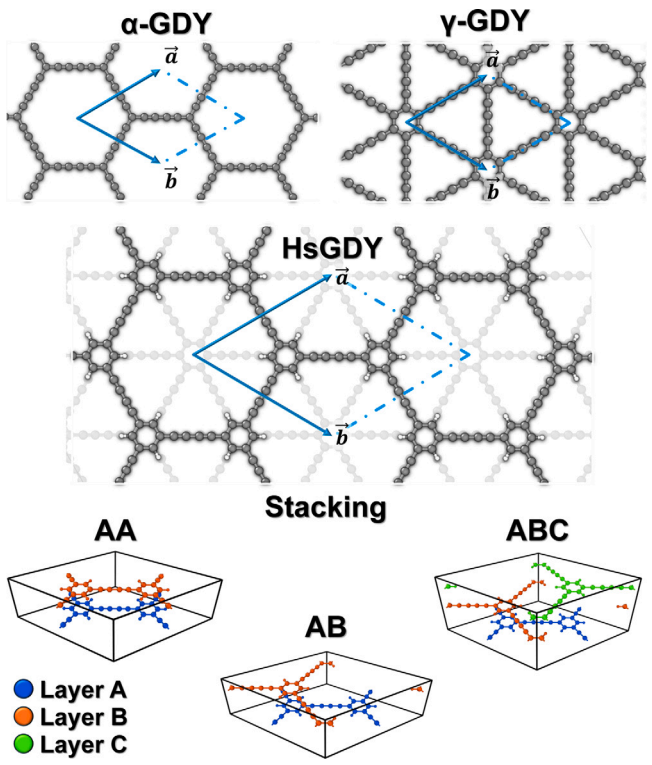

Fig. 1. Structural models illustrating the formation of HsGDY. The top panel compares the pristine α-GDY and γ-GDY networks with the HsGDY lattice, detailing the derivation of HsGDY by removing three alternating acetylenic linkages per hexagon, followed by passivation with hydrogen atoms. The bottom panels display the optimized structures of the layered HsGDY systems, highlighting the hexagonal in-plane lattice defined by the $\vec{a}$ and $\vec{b}$ vectors together with the AA, AB, and ABC stacking registries. Distinct colors label layers A, B, and C, which are used to emphasize the relative lateral offsets that differentiate the stacking sequences.

For α-GDY, structural optimization yields an in-plane hexagonal lattice with $a = b = 11.618$ Å, in very good agreement with previous theoretical works on this allotrope [10,15,35,36]. Within a single layer, the carbon network consists of benzene rings connected through diacetylenic linkages. Along the diacetylene chain, we obtain C–C distances of 1.261, 1.356, and 1.261 Å, while the C–C bond connecting adjacent chains is 1.415 Å. These values are consistent with the characteristic alternation of sp and sp^2 bond lengths reported for GDY frameworks [10,15]. Earlier studies of porous GDY sheets similarly report aromatic C–C distances near 1.42 Å, C=C bonds around 1.34 Å, and C≡C bonds close to 1.21–1.23 Å [10,15]. For γ-GDY, a similarly good agreement was obtained. The structural optimization yields an in-plane hexagonal lattice with a = b = 9.569 Å. Along the diacetylene chain, the calculated C–C bond lengths are 1.251, 1.359, and 1.251 Å, whereas the C–C bond linking adjacent chains is 1.415 Å, and those within the benzene ring are 1.442 Å.

HsGDY preserves the underlying hexagonal connectivity while incorporating out-of-plane C–H groups at selected aromatic sites, thereby enlarging the in-plane periodicity and modifying the local bonding environment. The primitive cell (one layer) contains six inequivalent atoms, four carbon and two hydrogen atoms, which generate a 30-atom hexagonal unit cell under the symmetry operations of the *P6/mmm* space group. The optimized lattice parameters for the AA-stacked crystal are $a = b = 16.63$ Å and $c = 6.82$ Å, in close agreement with values inferred from the experimental synthesis [18,19]. The larger in-plane periodicity is reflected in an increased pore diameter of 14.13 Å. At the hydrogenated aromatic sites, the optimized C–H bond length is 1.106 Å, consistent with values reported for hydrogenated graphdiyne films and porous graphene derivatives [37,38]. Aromatic C–C bonds within the rings are slightly elongated to 1.428 Å, whereas the diacetylene chain exhibits distances of 1.248, 1.373, and 1.248 Å, maintaining the expected alternation of triple and single or double bonds in mixed sp-sp^2 networks [37,38].

The comparison between α-GDY and HsGDY indicates that hydrogen substitution perturbs the local geometry without disrupting the global framework. While α-GDY remains essentially planar with nearly linear C–C–C angles along the diacetylene segments and an approximately trigonal sp^2 environment at the benzene rings, HsGDY exhibits small out-of-plane distortions at hydrogenated sites and a broader distribution of C–C–C angles in their vicinity. This behavior is consistent with a localized mixing of sp^2 and sp^3 character induced by C–H bonding.

The equilibrium interlayer spacing depends on the stacking registry. After full relaxation, AA, AB, and ABC configurations yield layer separations of 3.411, 3.273, and 3.252 Å, respectively, indicating that the laterally shifted AB and ABC arrangements allow a closer approach between neighboring HsGDY sheets. This trend reflects the interplay between dispersive π–π interactions, short-range Pauli repulsion arising from the vertical alignment of π orbitals, and steric effects associated with the out-of-plane C–H groups. The lateral offset reduces direct H–H and ring-ring overlap along the vertical direction, enabling a small contraction of the interlayer spacing while preserving the structural integrity of the porous framework.

A direct comparison with the experimental study of Liu et al. [18] shows that the relaxed AA structure reproduces the measured interlayer spacing of approximately 0.41 nm obtained from TEM and XRD analyses, and remains consistent with the pore dimensions inferred from BET and diffraction data. Small quantitative deviations in lattice parameters and bond lengths, typically within a few percent, are expected given the intrinsic differences between experimental and theoretical conditions. Experiments probe finite crystallites that may contain defects, residual functional groups, and environmental effects, whereas the present simulations describe ideal, defect-free crystals at zero temperature under periodic boundary conditions, using a nonlocal vdW functional. These comparisons support the view that the structural model adopted here captures the essential features of experimentally realized AA-stacked HsGDY while providing atomistic detail on bonding, stacking registry, and interlayer spacing that is difficult to extract directly from measurements.

3.2. Energy landscape

The energy stability of layered HsGDY was evaluated through cohesive and interlayer binding energies, which provide complementary measures of bulk thermodynamic robustness and stacking-driven stabilization. The cohesive energy per atom is defined as:

$$E_{\mathrm{coh}} = \frac{E_{\mathrm{bulk}} - \sum_i N_i E_i^{\mathrm{isol}}}{N_{\mathrm{tot}}}, \tag{1}$$

where E_{bulk} is the total energy of the crystalline phase, E_i^{isol} is the energy of an isolated atom of species i, N_i is the number of atoms of type i, and N_{tot} is the total number of atoms. The interlayer binding energy per atom is obtained from:

$$E_{\mathrm{bind}} = \frac{E_{\mathrm{stack}} - N_{\mathrm{layer}} E_{\mathrm{mono}}}{N_{\mathrm{tot}}}, \tag{2}$$

where E_{stack} is the total energy of the stacked structure, E_{mono} is the energy of a single isolated layer constrained to the same in-plane geometry, and N_{layer} is the number of layers in the stacking sequence.

To contextualize the thermodynamic stability of HsGDY, Fig. 2 compares its cohesive energy with those of α-GDY, graphite, and diamond, while also presenting the binding energies associated with distinct stacking registries.

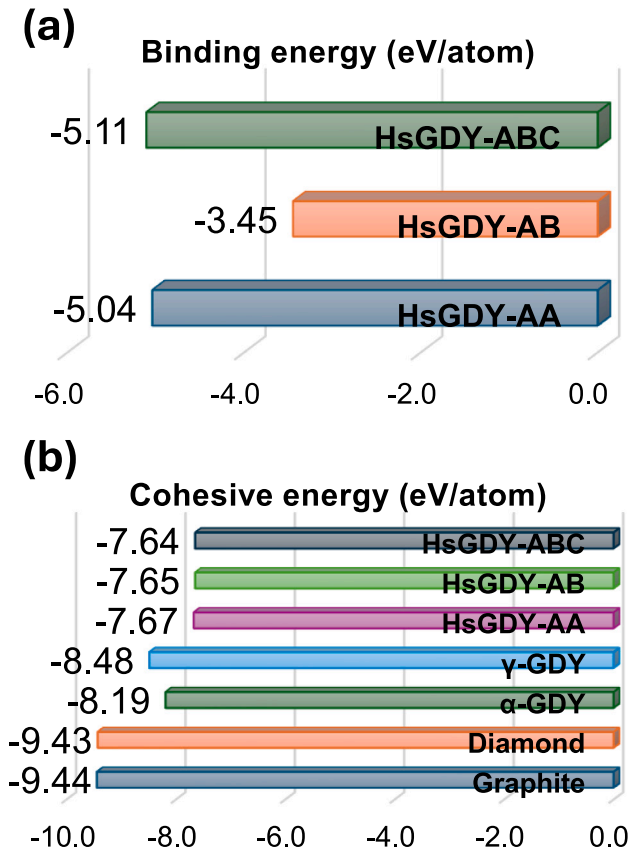

Fig. 2. HsGDY Energies. (a) Binding energy per atom for AA, AB, and ABC stacking sequences, highlighting the near degeneracy between AA and ABC and the reduced stability of the AB registry. (b) Cohesive energy per atom for graphite, diamond,γ-GDY, α-GDY, and HsGDY, positioning the hydrogenated framework within the stability spectrum of carbon allotropes.

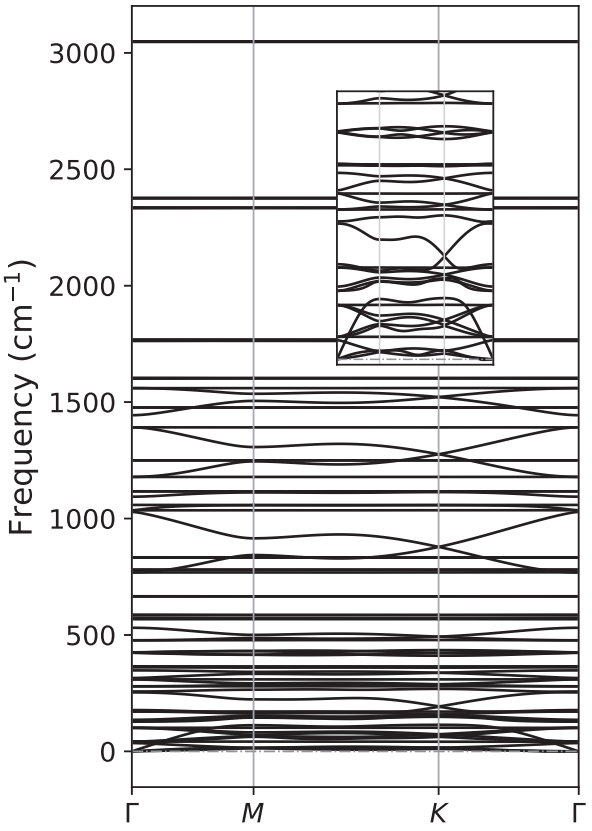

Fig. 3. Phononic band structure of bulk HsGDY.

The calculated cohesive energies follow the trend graphite < diamond < γ-GDY < α-GDY < HsGDY, with values of −9.44, −9.43, −8.48, −8.19, and −7.67 eV/atom, respectively. The lower values observed for the graphdiyne-derived frameworks reflect their porous architectures and mixed sp-sp^2 bonding, which result in lower atomic packing densities than the dense sp^2 and sp^3 networks of graphite and diamond.

A direct comparison between α-GDY and HsGDY reveals that hydrogen incorporation decreases the cohesive energy by approximately 0.5 eV/atom. It should be noted that the comparison between the cohesive energies of α-GDY and HsGDY must be interpreted with care. The introduction of hydrogen modifies both the bonding network and the total number of atoms used in the normalization of the cohesive energy. In addition, the presence of C–H bonds, which are generally weaker than C–C bonds, also contributes to the slightly smaller cohesive energy obtained for HsGDY. This decrease may originate from the partial replacement of extended C–C π conjugation by localized C–H σ-bonds, weakening the overall bonding network while preserving structural integrity. Such behavior aligns with previous studies on hydrogen-functionalized graphdiyne and related porous carbon frameworks.

The binding energy values indicate that AA and ABC configurations are nearly degenerate, with values of −5.04 and −5.11 eV/atom, whereas the AB stacking is markedly less stable at −3.45 eV/atom. The small energy difference between AA and ABC suggests that HsGDY accommodates multiple interlayer arrangements with comparable stabilization energies, indicating a relatively shallow energy landscape. By contrast, the energetic cost of AB stacking underscores the strong dependence of interlayer cohesion on lateral registry.

This behavior emerges from the interplay among dispersive π-π interactions, short-range Pauli repulsion arising from the vertical alignment of π orbitals, and steric effects introduced by the out-of-plane C–H groups. In AA and ABC configurations, the relative alignment between pores and hydrogenated sites promotes a more favorable balance among attractive dispersion forces, Pauli repulsion, and structural sterics. The AB arrangement, however, yields suboptimal overlap patterns, thereby weakening interlayer coupling. These findings indicate that hydrogen functionalization not only modifies local bonding but also reshapes the interlayer energy landscape that governs 3D stacking.

Although the nearest neighbor interlayer interactions are similar for the AB and ABC configurations, their bulk binding energies differ due to long-range van der Waals forces and the distinct registry of subsequent layers. Specifically, the ABC sequence avoids the direct vertical alignment of alternating layers in AB stacking, thereby altering extended electrostatic interactions and the overall packing efficiency of the 3D framework.

The present results are consistent with the experimental realization of AA-stacked HsGDY reported by Liu et al. [18], whose combined experimental and computational study first established this configuration as the preferred stacking sequence. Our calculations further support this stacking as most stable, while extending the analysis to alternative registries within a fully periodic framework, thereby providing a broader atomistic perspective on the interlayer energy landscape. Minor quantitative variations in the relative stacking energies are expected, given the different theoretical approaches and structural models employed. Importantly, both studies conclude that AA stacking is the most favorable configuration, highlighting the stabilizing role of ordered pore channels, as well as the interplay among dispersive π-π interactions, Pauli repulsion, and C–H-mediated steric effects in governing the assembly of the layered architecture.

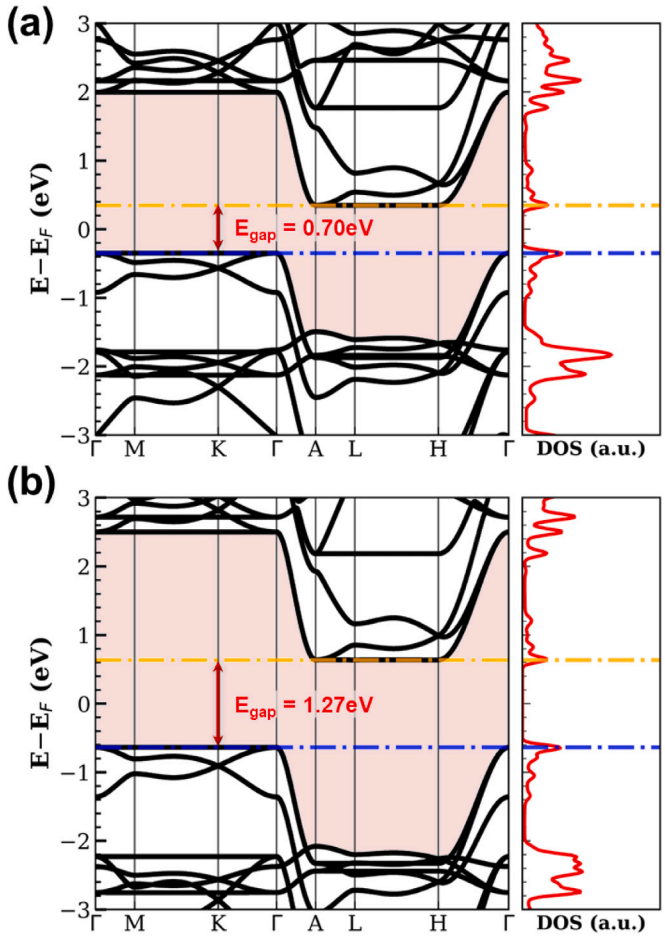

Fig. 4. Electronic band structures and the corresponding density of states (DOS) of AA-stacked bulk HsGDY calculated using (a) the vdW/KBM functional and (b) the HSE06 hybrid functional. The shaded region highlights the band gap, while the DOS identifies the carbon contributions near the band edges.

3.3. Dynamical and thermal stability

The structural robustness of layered HsGDY was further assessed through lattice dynamics and finite-temperature analyses. Fig. 3 presents the phonon dispersion of bulk HsGDY along the principal high-symmetry directions of the Brillouin zone.

The complete absence of imaginary frequencies demonstrates that HsGDY corresponds to a true minimum of the potential-energy surface and is therefore dynamically stable. The low-frequency region is dominated by acoustic and soft optical modes associated with interlayer shear and layer-breathing motions, indicating that the stacked architecture does not exhibit latent long-wavelength instabilities.

At higher frequencies, nearly dispersionless bands emerge as a characteristic feature of the vibrational spectrum. These flat modes originate predominantly from localized C–H vibrations together with stretching modes of the acetylenic C–C units, whose large force constants produce weakly dispersive phonons [39]. Such spectral separation provides clear vibrational fingerprints and reflects the coexistence of hydrogen functional groups with the rigid carbon backbone.

Thermal stability was further verified through AIMD simulations at 700 K. Throughout the simulation, the total energy fluctuated around approximately −126.819 eV/atom without a systematic drift, and no bond-breaking or bond-formation events were observed. The absence of structural degradation at this temperature indicates that the hydrogenated framework preserves its integrity under significant thermal excitation.

Taken together, the phonon spectrum and AIMD results consistently demonstrate that the HsGDY structures investigated here are both dynamically and thermally stable. These findings reinforce the energy landscape trends discussed previously and establish the layered hydrogen-substituted graphdiyne as a structurally robust 3D carbon framework suitable for applications requiring mechanical resilience and thermal reliability.

3.4. Electronic structure

The electronic band structures and the corresponding density of states (DOS) of AA-stacked bulk HsGDY are presented in Fig. 4, calculated with both the vdW/KBM and HSE06 functionals. To contextualize the effect of hydrogen substitution on the graphdiyne framework, the band structures of pristine α- and γ-GDY are provided in the Supplementary Material (Figure S1).

For α-GDY, the bands intersect at the Fermi level with a Dirac-like dispersion previously reported in the literature [10,35]. These linearly dispersive states originate predominantly from the C $2p_z$ orbitals belonging to the conjugated sp-sp^2 carbon network, confirming the semimetallic character associated with extended π delocalization.

In contrast, pristine γ-GDY behaves as a narrow-gap semiconductor with an estimated gap of 0.47–0.87 eV (Figure S1). As previously discussed, HsGDY can be structurally derived from the γ-GDY phase through the selective removal of acetylenic linkages and subsequent hydrogen passivation. This chemical modification significantly alters the electronic landscape, leading to a pronounced widening of the band gap.

AA-stacked HsGDY exhibits an indirect electronic band gap of approximately 0.70 eV at the vdW/KBM level. When evaluated with the

more accurate HSE06 hybrid functional, the gap increases to 1.27 eV, evidencing the electronic reconfiguration induced by hydrogen functionalization. The band-gap opening in HsGDY arises primarily from the modification of the π-conjugated carbon network and the associated symmetry breaking with respect to α- and γ-GDY. The DOS shows no hydrogen states, indicating that hydrogen functionalization mainly perturbs the carbon π system through structural confinement rather than directly forming the frontier states. Notably, the magnitude of this gap remains smaller when compared with fully hydrogenated graphene-derived materials, which typically display gaps between 1 and 4 eV [40–42], and with hydrogenated porous graphene networks that often reach values near 3.0–3.5 eV [43,44]. Functionalized graphdiyne monolayers may exhibit even larger gaps, approaching 5 eV, under extensive hydrogenation or halogenation [45]. The comparatively smaller gap found in HsGDY therefore indicates that the π-conjugated carbon network remains partially preserved, yielding a moderate-gap semiconductor rather than a strongly localized sp^3-dominated framework.

The DOS further clarifies the orbital origin of the frontier states. Within the evaluated low-energy window, the band edges are overwhelmingly dominated by C $2p_z$ contributions, demonstrating that the electronic response is governed entirely by the carbon π manifold. This behavior confirms that hydrogen acts primarily as an electronic perturbation of the carbon network, modifying conjugation without creating an independent carrier channel near the Fermi level.

Additional insights emerge when different stacking registries are compared. While AA-stacked HsGDY displays a vdW/KBM gap of 0.70 eV, the gap increases to 1.68 eV and 1.89 eV for the AB and ABC arrangements, respectively. This systematic gap widening reflects the sensitivity of the electronic structure to interlayer registry. Departures from the highly symmetric AA configuration reduce π-π overlap between adjacent layers, weaken band dispersion near the Fermi level, and shift the valence-band maximum and conduction-band minimum further apart in energy. Such behavior demonstrates that stacking provides an additional degree of freedom for tuning the electronic response of HsGDY beyond chemical functionalization alone.

These results reveal a clear transition from the Dirac semimetallicity of α-GDY to a stacking-dependent semiconducting regime in HsGDY. The coexistence of moderate band gaps with preserved π connectivity suggests a favorable balance between carrier transport and electronic controllability, positioning this hydrogen-substituted framework as a promising platform for optoelectronic and energy-related applications.

3.5. Optical properties

The anisotropic optical response of HsGDY was evaluated through the frequency-dependent absorption coefficient, refractive index, and reflectance along the crystallographic x, y, and z directions. Fig. 5 presents the spectra obtained for the AA-HsGDY, adopted here as the representative description of the bulk optical behavior.

The absorption spectra reveal a pronounced optical anisotropy. The in-plane components (x and y) exhibit intense features spanning the visible to near-UV regions, whereas the out-of-plane response remains significantly weaker throughout the investigated photon-energy range. This behavior directly reflects the layered architecture and the predominance of in-plane π conjugation, which enhances dipole-allowed transitions for light polarized parallel to the carbon backbone while suppressing vertical excitations.

The first strong absorption peaks emerge slightly above the fundamental electronic band gap, indicating that they originate primarily from direct interband transitions between frontier π states. These low-energy excitations are strongly governed by the specific orbital symmetry near the valence and conduction band edges. At higher photon energies, additional structures arise from transitions involving more dispersive π and σ bands, signaling the progressive participation of deeper valence states and higher conduction bands. This intense

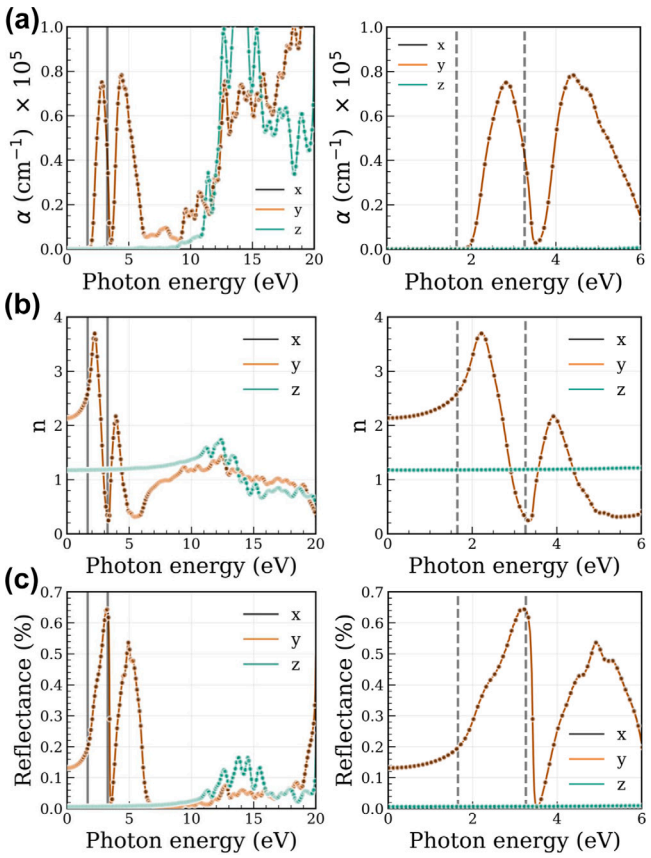

Fig. 5. Optical absorption coefficient, refractive index, and reflectance of HsGDY for the 30-atom unit cell along the x, y, and z directions. Dashed vertical lines indicate characteristic transition energies.

optical response in the visible spectrum is directly correlated with the delocalized nature of the extended carbon network. This spectral evolution is consistent with the previously discussed moderate band gap and confirms that hydrogen substitution preserves an electronically active carbon network rather than producing a strongly localized sp^3 framework.

The refractive index values follow the same directional trend. Larger static values are obtained for in-plane polarization, while the z component remains comparatively low, suggesting reduced optical confinement perpendicular to the layers. Reflectance remains moderate at low energies and increases near the main absorption peaks, indicating efficient light-matter coupling without the large metallic reflectivity typical of gapless systems. Collectively, these characteristics position HsGDY as a directional semiconductor with strong polarization selectivity.

To evaluate finite-size effects, the optical response was also computed for a 240-atom supercell that preserves the AA-stacked topology while extending the real-space periodicity of the porous framework. The spectral profiles remain essentially unchanged, with only minor energy shifts and slight intensity redistributions. No additional low-energy transitions appear, demonstrating that the primitive cell already captures the relevant local electronic environment and that artificial confinement effects are negligible at the scales considered.

These results establish that the optical behavior of bulk HsGDY is primarily governed by its anisotropic π network and stacking-preserved electronic structure. The coexistence of a moderate electronic band gap, strong in-plane absorption, and limited out-of-plane response suggests that hydrogen-substituted graphdiyne may serve as a promising platform for polarization-sensitive photodetectors, anisotropic optoelectronic components, and layered photonic architectures.

4. Conclusion and perspectives

In this work, we have performed a first-principles investigation of hydrogen-substituted graphdiyne (HsGDY), focusing on the influence of stacking configurations on its structural, electronic, and optical properties. Our results show that AA and ABC stackings are energetically favored, with AA corresponding to the global minimum, in agreement with recent experimental observations. The structures exhibit interlayer separations of approximately 3.3–3.4 Å, and both phonon dispersion and AIMD simulations confirm their dynamical and thermal stability. Electronic calculations reveal that AA-stacked HsGDY is an indirect semiconductor with a band gap of 0.70 eV dominated by C $2p_z$ states, while alternative stackings can further change the gap, highlighting interlayer registry as an effective control parameter. The optical response is strongly anisotropic, with intense in-plane absorption extending from the visible to the near-ultraviolet region. These findings provide atomistic insight into the stacking-dependent behavior of HsGDY and support its potential for optoelectronic and energy-related applications.

CRediT authorship contribution statement

Guilherme S.L. Fabris: Writing – original draft, Visualization, Software, Methodology, Investigation, Formal analysis, Data curation. **Raphael B. de Oliveira:** Writing – original draft, Software, Methodology, Investigation, Formal analysis, Data curation. **Bruno Ipaves:** Writing – original draft, Methodology, Investigation, Formal analysis. **Marcelo L. Pereira:** Writing – review & editing, Validation, Supervision, Software, Resources, Project administration, Methodology, Investigation, Funding acquisition, Formal analysis. **Douglas S. Galvão:** Writing – review & editing, Validation, Resources, Project administration, Investigation, Funding acquisition, Formal analysis, Conceptualization.

Declaration of competing interest

The authors declare that they have no known competing financial interests or personal relationships that could have appeared to influence the work reported in this paper.

Acknowledgments

Guilherme S. L. Fabris acknowledges the São Paulo Research Foundation (FAPESP) fellowship, Brazil (process number #2024/03413-9). Raphael B. de Oliveira thanks the National Council for Scientific and Technological Development (CNPq), Brazil (process numbers 151043/2024-8 and 200257/2025-0). Bruno Ipaves thanks CNPq, Brazil process number #194155/2025-0 and FAPESP, Brazil process numbers #2024/11016-0. Marcelo L. Pereira Junior acknowledges financial support from FAPDF, Brazil (grant 00193-00001807/2023-16), CNPq, Brazil (grants 444921/2024-9 and 308222/2025-3), and CAPES, Brazil (grant 88887.005164/2024-00). Douglas S. Galvão acknowledges the Center for Computing in Engineering and Sciences at Unicamp for financial support through the FAPESP/CEPID Grant (process number #2013/08293-7). We thank the Coaraci Supercomputer Center for computer time (process number #2019/17874-0). Douglas S. Galvao also acknowledges support from INEO/CNPq and FAPESP, Brazil grant 2025/27044-5.

Appendix A. Supplementary data

Supplementary material related to this article can be found online at https://doi.org/10.1016/j.diamond.2026.113687.

Data availability

Data will be made available on request.

References

[1] A.K. Geim, K.S. Novoselov, The rise of graphene, Nat. Mater. 6 (3) (2007) 183–191.
[2] Q. Peng, A.K. Dearden, J. Crean, L. Han, S. Liu, X. Wen, S. De, New materials graphyne, graphdiyne, graphone, and graphane: review of properties, synthesis, and application in nanotechnology, Nanotechnol. Sci. Appl. 7 (2014) 1–29, http://dx.doi.org/10.2147/NSA.S40324.
[3] R. Paupitz, A.F. Fonseca, M. Bessa, G.S. Fabris, W.F. da Cunha, L.D. Machado, M.P. Junior, L.R. Junior, D.S. Galvão, A concise review of recently synthesized 2d carbon allotropes: Amorphous carbon, graphynes, biphenylene and fullerene networks, Carbon (2026) 121320.
[4] K.S. Novoselov, A.K. Geim, S.V. Morozov, D.-e. Jiang, Y. Zhang, S.V. Dubonos, I.V. Grigorieva, A.A. Firsov, Electric field effect in atomically thin carbon films, Science 306 (5696) (2004) 666–669.
[5] R. Baughman, H. Eckhardt, M. Kertesz, Structure-property predictions for new planar forms of carbon: Layered phases containing sp 2 and sp atoms, J. Chem. Phys. 87 (11) (1987) 6687–6699.
[6] Q. Li, Y. Li, Y. Chen, L. Wu, C. Yang, X. Cui, Synthesis of γ-graphyne by mechanochemistry and its electronic structure, Carbon 136 (2018) 248–254.
[7] V.G. Desyatkin, W.B. Martin, A.E. Aliev, N.E. Chapman, A.F. Fonseca, D.S. Galvão, E.R. Miller, K.H. Stone, Z. Wang, D. Zakhidov, F.T. Limpoco, S.R. Almahdali, S.M. Parker, R.H. Baughman, V.O. Rodionov, Scalable synthesis and characterization of multilayer γ-graphyne, new carbon crystals with a small direct band gap, J. Am. Chem. Soc. 144 (39) (2022) 17999–18008, http://dx.doi.org/10.1021/jacs.2c06583, PMID: 36130080.
[8] A.E. Aliev, Y. Guo, A.F. Fonseca, J.M. Razal, Z. Wang, D.S. Galvão, C.M. Bolding, N.E. Chapman-Wilson, V.G. Desyatkin, J.E. Leisen, L.A.R. Junior, G.B. Kanegae, P. Lynch, J. Zhang, M.A. Judicpa, A.M. Parra, M. Zhang, E. Gao, L. Hu, V.O. Rodionov, R.H. Baughman, A planar-sheet nongraphitic zero-bandgap sp^2 carbon phase made by the low-temperature reaction of γ-graphyne, Proc. Natl. Acad. Sci. 122 (5) (2025) e2413194122, http://dx.doi.org/10.1073/pnas.2413194122.
[9] G. Li, Y. Li, H. Liu, Y. Guo, Y. Li, D. Zhu, Architecture of graphdiyne nanoscale films, Chem. Commun. 46 (19) (2010) 3256–3258.
[10] C. Huang, Y. Li, N. Wang, Y. Xue, Z. Zuo, H. Liu, Y. Li, Progress in research into 2D graphdiyne-based materials, Chem. Rev. 118 (16) (2018) 7744–7803, http://dx.doi.org/10.1021/acs.chemrev.8b00288.
[11] V. Coluci, S. Braga, S. Legoas, D. Galvao, R. Baughman, Families of carbon nanotubes: Graphyne-based nanotubes, Phys. Rev. B 68 (3) (2003) 035430.
[12] V. Coluci, S. Braga, S. Legoas, D. Galvao, R. Baughman, New families of carbon nanotubes based on graphyne motifs, Nanotechnology 15 (4) (2004) S142.
[13] D.A. Solis, D. D. Borges, C.F. Woellner, D.S. Galvão, Structural and thermal stability of graphyne and graphdiyne nanoscroll structures, ACS Appl. Mater. Interfaces 11 (3) (2019) 2670–2676, http://dx.doi.org/10.1021/acsami.8b03481, arXiv:https://doi.org/10.1021/acsami.8b03481.
[14] M. Long, L. Tang, D. Wang, Y. Li, Z. Shuai, Electronic structure and carrier mobility in graphdiyne sheet and nanoribbons: theoretical predictions, ACS Nano 5 (4) (2011) 2593–2600.
[15] X. Zheng, S. Chen, J. Li, H. Wu, C. Zhang, D. Zhang, X. Chen, Y. Gao, F. He, L. Hui, et al., Two-dimensional carbon graphdiyne: advances in fundamental and application research, ACS Nano 17 (15) (2023) 14309–14346.
[16] Y. Zhao, L. Chai, X. Yan, W. Huang, T. Fan, O.A. Al-Hartomy, A. Al-Ghamdi, S. Wageh, A.G. Al-Sehemi, Z. Xie, H. Zhang, Characteristics, properties, synthesis and advanced applications of 2D graphdiyne versus graphene, Mater. Chem. Front. 6 (4) (2022) 528–552, http://dx.doi.org/10.1039/D1QM01657F.
[17] X. Dang, H. Zhao, Graphdiyne: A promising 2D all-carbon nanomaterial for sensing and biosensing, Trends Anal. Chem. 137 (2021) 116194, http://dx.doi.org/10.1016/j.trac.2021.116194.
[18] Y. Liu, Z. Chen, C. Lai, X. Li, Z. Qu, C. Li, M. Peng, H. Fan, F. Ding, L. Zhang, AA-stacked hydrogen-substituted graphdiyne for enhanced lithium storage, Angew. Chem. 137 (14) (2025) e202422089.
[19] F. Kang, W. Zheng, L. Sun, W. Gao, L. Shang, L. Chi, W. Xu, On-surface synthesis of hydrogen-substituted γ-graphdiyne with high efficiency, CCS Chem. 6 (11) (2024) 2644–2651.
[20] W. Kohn, L.J. Sham, Self-consistent equations including exchange and correlation effects, Phys. Rev. 140 (4A) (1965) A1133.
[21] J.M. Soler, E. Artacho, J.D. Gale, A. García, J. Junquera, P. Ordejón, D. Sánchez-Portal, The SIESTA method for ab initio order-Nmaterials simulation, J. Phys.: Condens. Matter. 14 (11) (2002) 2745.
[22] A. García, N. Papior, A. Akhtar, E. Artacho, V. Blum, E. Bosoni, P. Brandimarte, M. Brandbyge, J.I. Cerdá, F. Corsetti, et al., Siesta: Recent developments and applications, J. Chem. Phys. 152 (20) (2020) 204108.
[23] J. Klimeš, D.R. Bowler, A. Michaelides, Chemical accuracy for the van der Waals density functional, J. Phys.: Condens. Matter. 22 (2) (2009) 022201, http://dx.doi.org/10.1088/0953-8984/22/2/022201.
[24] D. Bennett, M. Pizzochero, J. Junquera, E. Kaxiras, Accurate and efficient localized basis sets for two-dimensional materials, Phys. Rev. B 111 (12) (2025) 125123.
[25] H.J. Monkhorst, J.D. Pack, Special points for Brillouin-zone integrations, Phys. Rev. B 13 (12) (1976) 5188.

[26] J. Heyd, G.E. Scuseria, M. Ernzerhof, Hybrid functionals based on a screened Coulomb potential, J. Chem. Phys. 118 (18) (2003) 8207–8215, http://dx.doi.org/10.1063/1.1564060.
[27] X. Qin, H. Shang, H. Xiang, Z. Li, J. Yang, HONPAS: A linear scaling open-source solution for large system simulations, Int. J. Quantum Chem. 115 (10) (2015) 647–655, http://dx.doi.org/10.1002/qua.24837.
[28] H. Shang, L. Xu, B. Wu, X. Qin, Y. Zhang, J. Yang, The dynamic parallel distribution algorithm for hybrid density-functional calculations in HONPAS package, Comput. Phys. Comm. 254 (2020) 107204, http://dx.doi.org/10.1016/j.cpc.2020.107204.
[29] D.J. Evans, B.L. Holian, The nose–hoover thermostat, J. Chem. Phys. 83 (8) (1985) 4069–4074.
[30] M. Elstner, D. Porezag, G. Jungnickel, J. Elsner, M. Haugk, T. Frauenheim, S. Suhai, G. Seifert, Self-consistent-charge density-functional tight-binding method for simulations of complex materials properties, Phys. Rev. B 58 (11) (1998) 7260–7268, http://dx.doi.org/10.1103/PhysRevB.58.7260, URL http://link.aps.org/doi/10.1103/PhysRevB.58.7260.
[31] B. Hourahine, B. Aradi, V. Blum, F. Bonafé, A. Buccheri, C. Camacho, C. Cevallos, M.Y. Deshaye, T. Dumitrică, A. Dominguez, S. Ehlert, M. Elstner, T. van der Heide, J. Hermann, S. Irle, J.J. Kranz, C. Köhler, T. Kowalczyk, T. Kubař, I.S. Lee, V. Lutsker, R.J. Maurer, S.K. Min, I. Mitchell, C. Negre, T.A. Niehaus, A.M.N. Niklasson, A.J. Page, A. Pecchia, G. Penazzi, M.P. Persson, J. Řezáč, C.G. Sánchez, M. Sternberg, M. Stöhr, F. Stuckenberg, A. Tkatchenko, V.W. z. Yu, T. Frauenheim, DFTB+, a software package for efficient approximate density functional theory based atomistic simulations, J. Chem. Phys. 152 (12) (2020) 124101, http://dx.doi.org/10.1063/1.5143190.
[32] G. Zheng, S. Irle, K. Morokuma, Performance of the DFTB method in comparison to DFT and semiempirical methods for geometries and energies of C-20-C-86 fullerene isomers, Chem. Phys. Lett. 412 (1-3) (2005) 210–216, http://dx.doi.org/10.1016/j.cplett.2005.06.105.
[33] B. Hourahine, M. Berdakin, J.A. Bich, F.P. Bonafé, C. Camacho, Q. Cui, M.Y. Deshaye, G. Díaz Mirón, S. Ehlert, M. Elstner, T. Frauenheim, N. Goldman, R.A. González León, T. van der Heide, S. Irle, T. Kowalczyk, T. Kubař, I.S. Lee, C.R. Lien-Medrano, A. Maryewski, T. Melson, S.K. Min, T. Niehaus, A.M.N. Niklasson, A. Pecchia, K. Reuter, C.G. Sánchez, C. Scheurer, M.A. Sentef, P.V. Stishenko, V.Q. Vuong, B. Aradi, Recent developments in DFTB+, a software package for efficient atomistic quantum mechanical simulations, J. Phys. Chem. A 129 (24) (2025) 5373–5390, http://dx.doi.org/10.1021/acs.jpca.5c01146.
[34] A. Togo, L. Chaput, T. Tadano, I. Tanaka, Implementation strategies in phonopy and phono3py, J. Phys.: Condens. Matter. 35 (35) (2023) 353001.
[35] X. Niu, X. Mao, D. Yang, Z. Zhang, M. Si, D. Xue, Dirac cone in α-graphdiyne: a first-principles study, Nanoscale Res. Lett. 8 (1) (2013) 469.
[36] L. Li, W. Qiao, H. Bai, Y. Huang, Structural and electronic properties of α-, β-, γ-, and 6, 6, 18-graphdiyne sheets and nanotubes, RSC Adv. 10 (28) (2020) 16709–16717, http://dx.doi.org/10.1039/d0ra01777a.
[37] H. Qiu, X. Sheng, A first principle study of hydrogenated graphdiyne, Phys. Lett. A 382 (9) (2018) 662–666.
[38] H. Lee, J. Koo, M. Capone, Y. Kwon, H. Lee, DFT and TB study of the geometry of hydrogen adsorbed on graphynes, J. Phys.: Condens. Matter. 26 (38) (2014) 385301.
[39] T. Jenkins, A.M. Silva, M.G. Menezes, T. Thonhauser, S. Ullah, Thd-c sheet: A novel nonbenzenoid carbon allotrope with tetra-, hexa-, and dodeca-membered rings, J. Phys. Chem. C 128 (26) (2024) 10982–10996.
[40] D. Haberer, D.V. Vyalikh, S. Taioli, B. Dora, M. Farjam, J. Fink, D. Marchenko, T. Pichler, K. Ziegler, S. Simonucci, M.S. Dresselhaus, M. Knupfer, B. Büchner, A. Grüneis, Tunable band gap in hydrogenated quasi-free-standing graphene, Nano Lett. 10 (9) (2010) 3360–3366, http://dx.doi.org/10.1021/nl101066m.
[41] J.O. Sofo, A.S. Chaudhari, G.D. Barber, Graphane: A two-dimensional hydrocarbon, Phys. Rev. B—Condens. Matter Mater. Phys. 75 (15) (2007) 153401.
[42] J. Son, S. Lee, S.J. Kim, B.C. Park, H.-K. Lee, S. Kim, J.H. Kim, B.H. Hong, J. Hong, Hydrogenated monolayer graphene with reversible and tunable wide band gap and its field-effect transistor, Nat. Commun. 7 (1) (2016) 13261.
[43] G.S. Fabris, C.E. Junkermeier, R. Paupitz, Porous graphene and graphenylene nanotubes: Electronic structure and strain effects, Comput. Mater. Sci. 140 (2017) 344–355, http://dx.doi.org/10.1016/j.commatsci.2017.09.009.
[44] G. Fabris, N. Marana, E. Longo, J. Sambrano, Theoretical study of porous surfaces derived from graphene and boron nitride, J. Solid State Chem. 258 (2018) 247–255, http://dx.doi.org/10.1016/j.jssc.2017.10.025.
[45] J. Koo, M. Park, S. Hwang, B. Huang, B. Jang, Y. Kwon, H. Lee, Widely tunable band gaps of graphdiyne: an ab initio study, Phys. Chem. Chem. Phys. 16 (19) (2014) 8935–8939, http://dx.doi.org/10.1039/c4cp00800f.